ELSEVIER

Journal of Materials Processing Technology 141 (2003) 93–100

Journal of Materials Processing Technology

www.elsevier.com/locate/jmatprotec

Chemical and structural characterization of the crystalline phases in agglomerated fluxes for submerged-arc welding

Ana Ma. Paniagua-Mercado[a,b,*], Paulino Estrada-Diaz[c], Victor M. López-Hirata[a]

[a]*Instituto Politécnico Nacional (ESIQIE), Apartado Postal 75-395, Mexico D.F. 07300, Mexico*
[b]*Centro de Asimilación Tecnológica-FESC, Universidad Nacional Autónoma de México, Cuautitlan, Edo. Mex., Mexico*
[c]*POSSEHL S.A. de C.V., Cuautitlan, Edo. Mex., Mexico*

Received 3 January 2002; received in revised form 7 June 2002; accepted 8 January 2003

Abstract

A study of chemical and structural characterization of fluxes for submerged-arc welding was conducted. Three flux formulations were prepared using mineral oxides for agglomerating and sintering processes. A commercial agglomerated and sintered flux was used for comparison. The four fluxes were analyzed chemically by atomic absorption and X-ray diffraction to determinate the quantity and type of oxides formed, as well as the change in oxidation number after the sintering process at 950 °C of the initial compounds. Differential thermal analysis was carried out from 1000 to 1350 °C in order to determine the temperatures for phase transformations and melting of the different compounds formed in the sintering process.

This kind of flux characterization enables us to quantify the ions that might be present in the plasma arc during the submerged welding process due to the fluxes. This analysis also make possible the prediction of reactions in the weld pool.

Keywords: Crystalline phases; Agglomerated fluxes; Submerged-arc welding

1. Introduction

The weld metal chemistry is affected by the electrochemical reaction at the weld pool flux interface. The main characteristics of submerged-arc welds are a function of the fluxes and their physicochemical properties [1].

Submerged-arc welding (SAW) fluxes are manufactured in three main forms; fused at temperatures exceeding 1400 °C, agglomerated from 400 to 900 °C and sintered from 1000 to 1100 °C from mineral constituents [2].

Reactions, which occur during firing of a ceramic oxide, comprise phase transformations of minerals [3], reaction among the different phases [4], formation of crystal phases from the melt [5] and formation of a melt [4].

The phase transformation of the crystal phases predominates at the early stages of firing, before a melt is formed. The formation of a melt can be observed at temperatures as low as 920 °C, due to the presence of minor amounts of impurities such as, alkaline earth oxides [6]. In this way, the agglomerated fluxes can be studied by the chemical analysis of the crystal phases formed during the increase of temperature. This enables us to quantify types of ions and their distribution, which is useful to predict their behavior when they are dissociated in the SAW process [7].

Thus, the purpose of this work is to carry out a study of the crystalline phases and the chemical characterization of the ions formed in agglomerated fluxes using chemical analysis, X-ray diffraction (XRD) and differential thermal analysis (DTA). It is also intended to show the effect of ion content of flux on the behavior of SAW.

2. Experimental procedure

Three agglomerated welding fluxes were prepared, using mixtures of mineral oxides in different proportions (designated as A, B and C), as shown in Table 1. Each mixture was weighed, mixed in a vibratory camera for 30 min and subsequently pelletized in a laboratory machine of 80 cm diameter and 28 cm height at 40 rpm, using sodium silicate as the agglomerate agent. The average size of pellets was 5 mm. They were dried in a stove at 200 °C for 24 h, fired for 3 h at 950 °C in a gas kiln at a heating rate of 50 °C/h, crushed and then screened to a 240 μm size. For comparison, a commercial agglomerated welding flux was also used, designated as T sample. The chemical analysis was determined by X-ray fluorescence. The XRD analysis was conducted in a

* Corresponding author. Present address: Instituto Politécnico Nacional (ESIQIE), Apartado Postal 75-395, Mexico D.F. 07300, Mexico.

0924-0136/$ – see front matter
doi:10.1016/S0924-0136(03)00155-9

Table 1
Initial composition of fluxes

Compounds (wt.%)	Flux A	Flux B	Flux C
Al_2O_3	2.6	8	8
SiO_2	43.8	25	20
Fe_2O_3	6	2	9
K_2O	0.11	0.07	0.07
Na_2CO_3	0.09	1	0.20
$CaCO_3$	20	3	5
MnO	7	–	11
MgO	6	1	5
TiO_2	10	29	31

Table 3
Oxide compound of fused fluxes

Oxide (wt.%)	Flux A	Flux B	Flux C	Flux T
Al_2O_3	7.29	23	23	18.36
SiO_2	54.65	31.50	24.50	11.69
Fe_2O_3	2.48	0.74	3.92	3.43
K_2O	0.44	0.28	0.28	0.38
Na_2O	1.41	14	3.18	1.21
CaO	11.33	1.69	2.63	6.78
MnO	5.30	–	8.23	11.88
MgO	4.64	0.61	4.12	7.41
TiO_2	9	26	28	36.31

diffractometer with a monochromated Cu Kα radiation. For all the samples, the DTA analysis was carried out in a Al_2O_3 crucible from 25 to 1350 °C at a heating rate of 10 °C/min. Alumina was used as standard reference for DTA analysis.

3. Results and discussion

3.1. Chemical analysis

Table 2 shows the elemental chemical composition of the mixtures A, B and C, calculated with the data shown in Table 1 and the stequiometric formula of each compound. Tables 3 and 4 show the elemental chemical analysis and oxide compounds, respectively, for the fused fluxes A, B, C and T.

Table 2
Elemental chemical analysis of fused fluxes

Element (wt.%)	Flux A	Flux B	Flux C	Flux T
Al	3.85	12.17	12	9.71
Si	25.53	14.72	11.47	5.46
Fe	1.74	0.52	2.74	2.4
K	0.37	0.24	0.24	0.32
Na	1.05	10.4	2.36	0.9
Ca	8.1	1.21	1.88	4.85
Mn	4.11	–	6.38	9.2
Mg	2.8	0.37	2.49	4.47
C	0.46	0.53	0.03	0.08
S	0.08	0.028	0.06	0.016
Ti	5.3	15.5	16.7	21.6

By comparison of Table 1 with Table 3, it can be noticed that there was an increase in the percentage of Al_2O_3, SiO_2, and Na_2O. These oxides increased at the same proportion as they were present in the original mixtures. This can be attributed to the evaporation of impurities such as alkaline oxides with a low melting point that were present in the original mineral [6]. The amount of CaO showed the highest decrease because it came from the $CaCO_3$ compound, in the original mixture, which is decomposed at about 900 °C [3]. The Na_2O is also formed from Na_2CO_3, but its proportion is a little higher than the original one because the sodium silicate, Na_2SiO_4 was used for the agglomerating process. In order to be agglomerated, a higher amount of sodium silicate was added to the flux B than that added to the fluxes A and C. This fact explains the difference in Na_2O composition.

In the SAW process, the temperature of electric arc causes the dissociation of oxides and these remains as ions in the plasma [8]. The temperature in the welding pool reaches 1560–2300 °C. Christensen and Gjermundsen [9] calculated temperatures above 2500 °C for the welding pool in mild steels. Apold [10] suggested that the heat energy provided by the electric arc is concentrated on a circumference of 5 mm diameter. According to the above information, most of the

Table 4
Weight percent of compounds determined from XRD

Name	Composition	A	B	C	T
Corundum	Al_2O_3	9.17	17.90	12.11	19.07
Quartz	SiO_2	51.10	17.05	18.38	6.90
Nepheline	$NaAlSiO_4$	12.65	19.95	17.12	–
Gismodine	$CaAl_2Si_2O_8{\cdot}4H_2O$	12.65	–	–	–
Vesuvianite	$Ca_{19}Al_{11}Mg_2Si_{18}O_{69}(OH)_9$	–	10.23	–	–
Hausmannite	$Mn_3O_4[MnOMnO_2O_3]$	5.24	3.80		6.10
Anastase	TiO_2	–	6.95	3.60	53.03
Rutile	TiO_2	9.17	–	–	–
γ-Titanium oxide	Ti_3O_5	–	20.32	–	–
Titanium oxide	Ti_2O_3	–	–	25.65	–
Manganese oxide	Mn_2O_3	–	–	8.55	–
Calcium oxide	CaO			3.56	
Fluorite	CaF_2	–	–	–	14.90

oxides are melted, but oxides with high melting points such as MgO (2500–2800 °C), CaO (2572 °C) and ZrO_2 (2720 °C) are not melted. That is, it is important that the chemical formulation of fluxes enables all the oxides to be melted in order to avoid the presence of inclusion in the weldment.

3.2. XRD analysis

Figs. 1–4 shows the XRD patterns of agglomerated and sintered fluxes. Here, it can be observed the presence of crystalline phases, such as Nepheline ($NaAlSiO_4$), Gismodine ($CaAl_2Si_2O_8{\cdot}4H_2O$) and Vesuvianite ($Ca_{19}Al_{11}Mg_2Si_{18}O_{69}(OH)_9$), which were formed at low temperature [11]. These are equilibrium phases and were formed due to the reaction at the sintered temperature between different ions of the original mixture with the sodium silicate, added during the agglomeration process. Other oxides, such as titanium oxide and manganese oxide showed practically no reaction with other reactants at these temperature; however, they appeared with a different oxidation degree and crystalline structure. The silicon oxide, aluminum oxide and calcium oxide did not react at all.

The Nepheline phase can be formed by replacement of the half of silicon atoms with aluminum atoms in the sodium silicate compound [12]. The electric balance is kept by the addition of sodium ions in the interstitial sites of the hexagonal structure [11]. Its quantification is shown in Table 4 and it was based on the XRD peaks with the highest intensity [13]. Table 5 shows the quantification of ions calculated according to its disassociation reaction at the temperature of electric arc, as proposed by Davis and Bailey [14].

The Gismodine phase can be melted at low temperatures and has a monoclinic structure and also appeared in the sintered fluxes. The quantification of compound and ions is shown in Tables 4 and 5, respectively.

The Vesuvianite phase has a low melting point and tetragonal crystalline structure. This could be formed by means of the replacement of aluminum with silicon. This phase has also a low melting temperature and a tetragonal structure. Its quantification is also shown in Tables 4 and 5. The other detected phases were quartz, rutile, anastase and γ-titanium oxide. Fluorite was only detected in the flux T. All these compounds showed practically no reaction at the sintering temperature. These were also stable at room temperature. Tables 4 and 5 show their quantification as ions and compounds, respectively.

The formation of different oxides and silicates observed in fluxes A, B and C, but not in flux T can be attributed to the addition of sodium silicate used in the agglomeration process of the former fluxes, as well as the high sintering temperature.

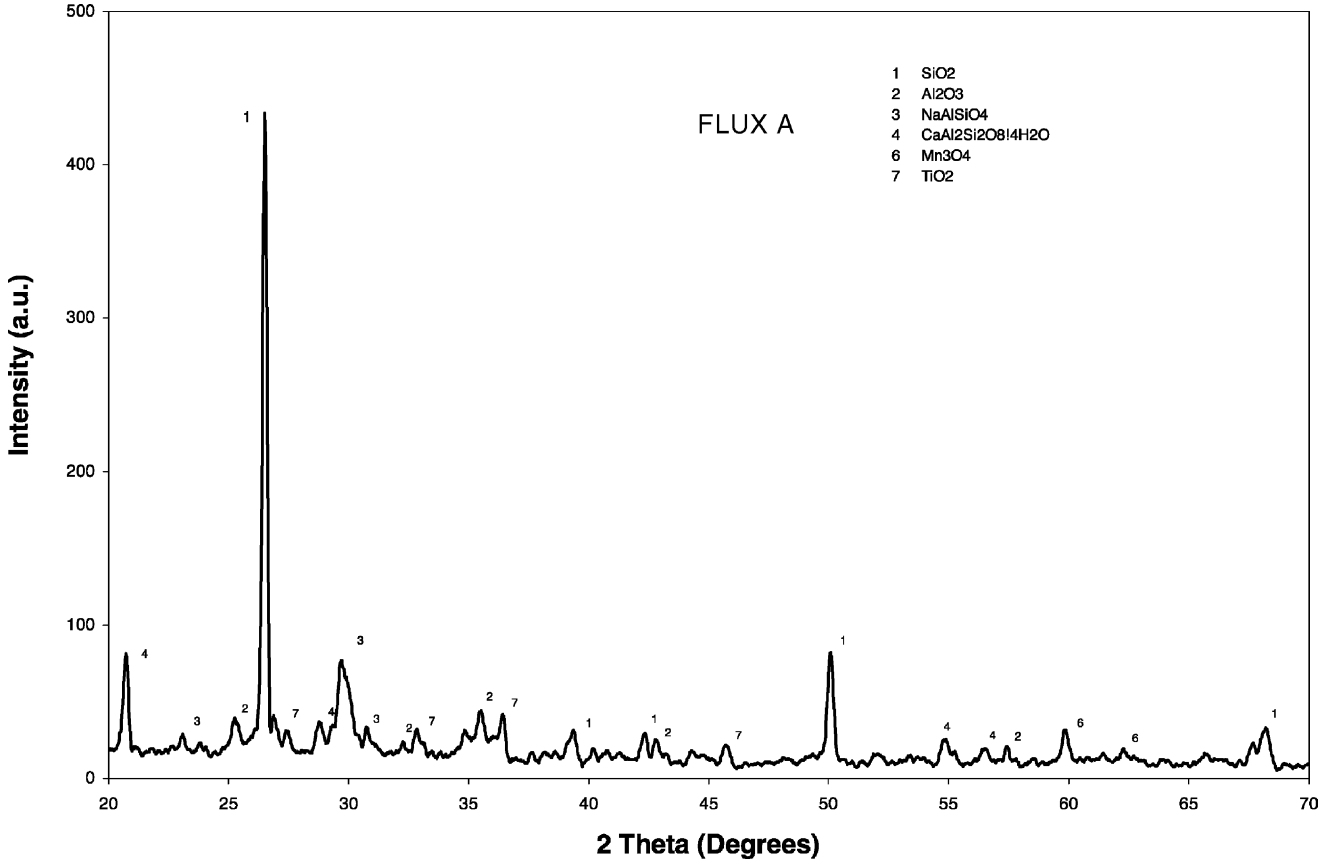

Fig. 1. XRD pattern of the flux A.

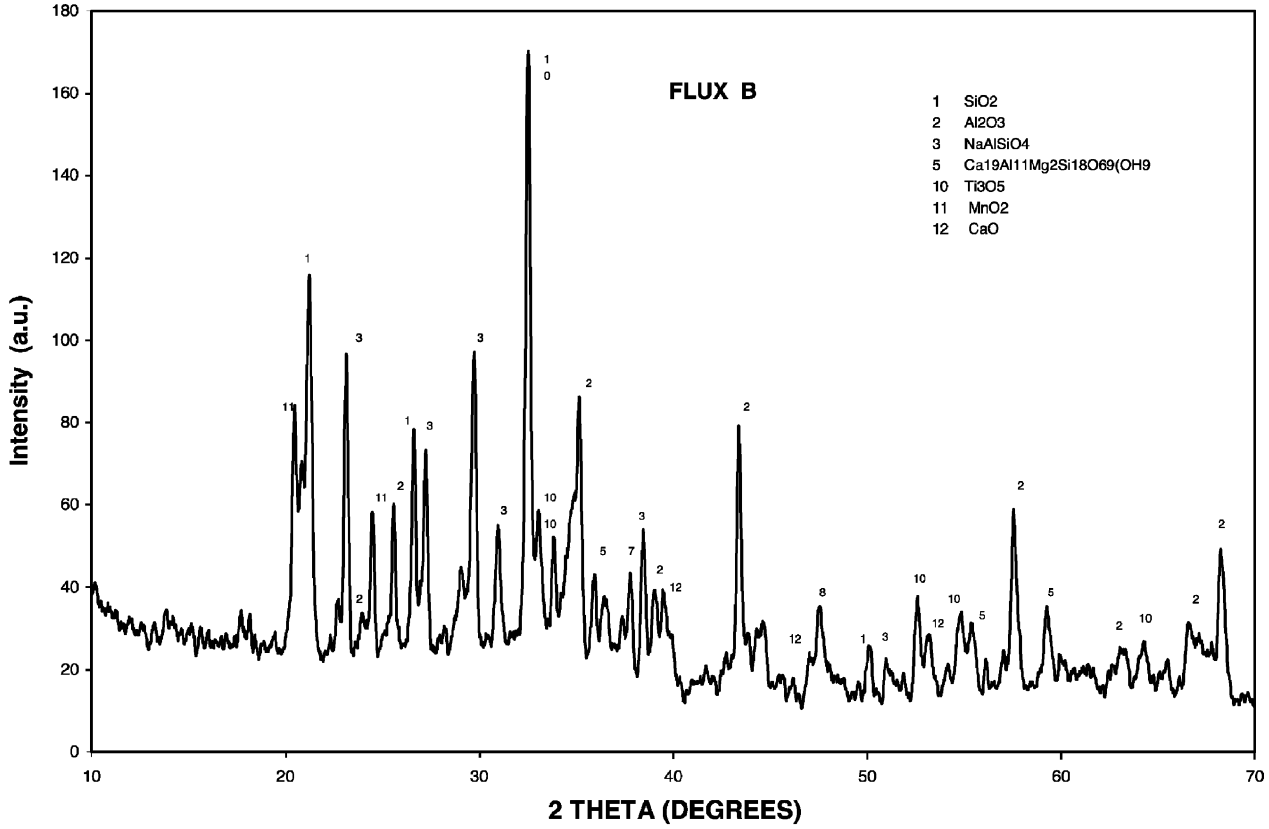

Fig. 2. XRD pattern of the flux B.

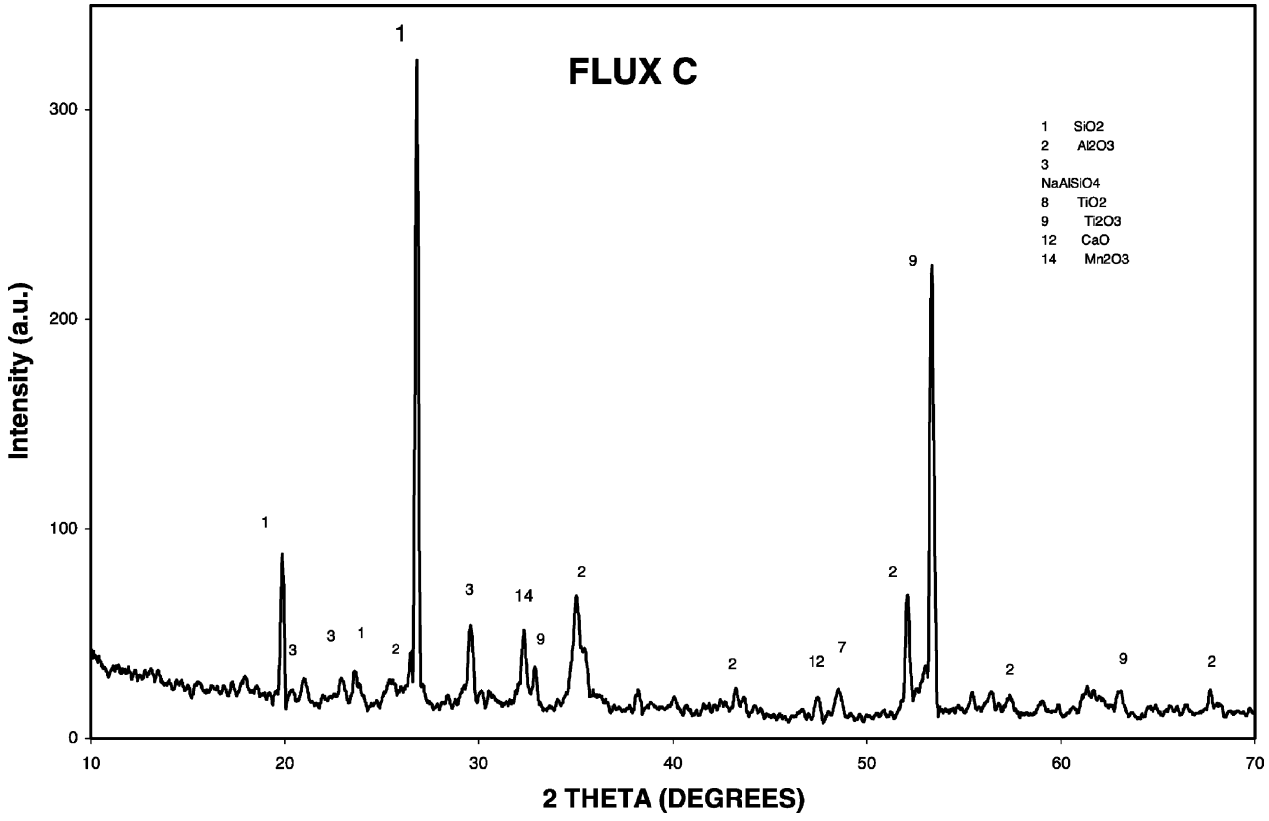

Fig. 3. XRD pattern of the flux C.

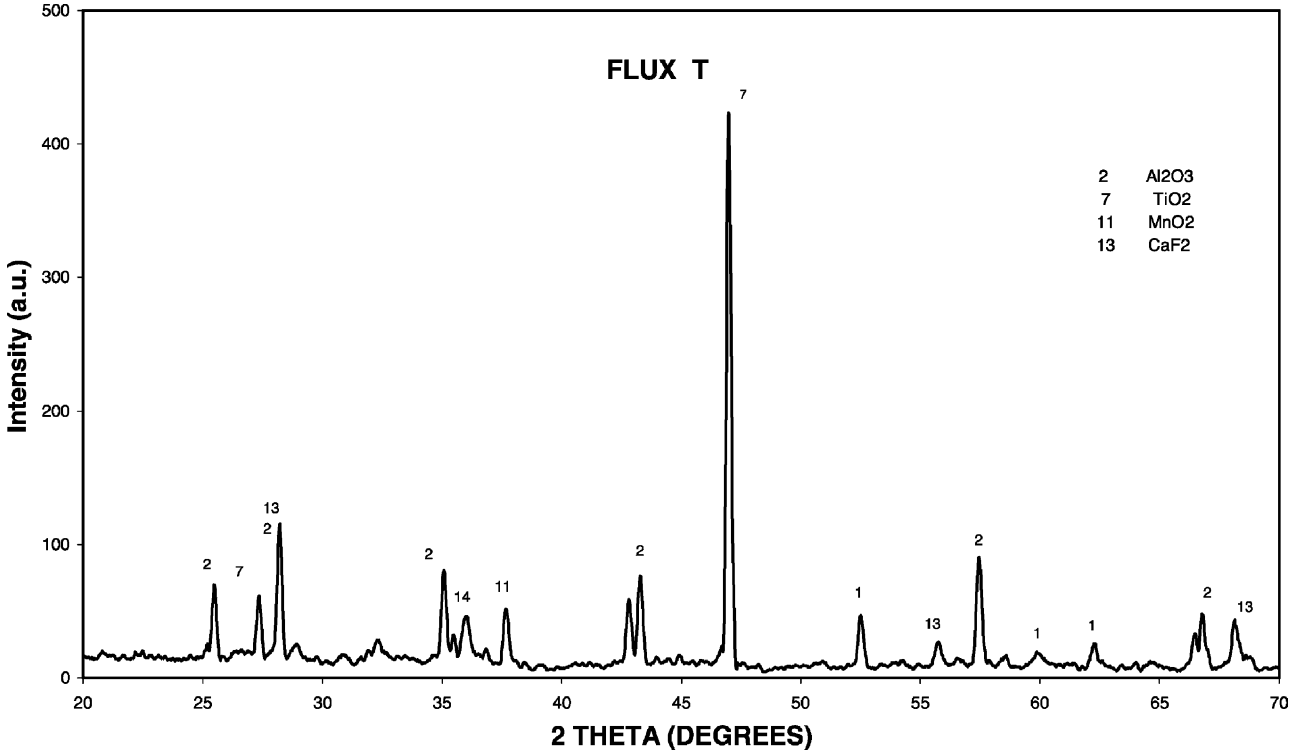

Fig. 4. XRD pattern of the flux T.

3.3. Differential thermal analysis

All oxides were stable during heating of DTA up to 1000 °C. Thus, the DTA curves are shown in the range of 1000–1350 °C for fluxes A, B, C and T in Figs. 5–8, respectively. Most of the reactions observed in DTA curves were endothermic type. Some of the endothermic peaks are located at close temperature values for the different fluxes. For instance, an endothermic peak is located at 1147.8, 1121.4, 1122.3 and 1161.6 °C for the fluxes A, B, C and T, respectively. Another one is located at 1226, 1189.3, 1213.4 and 1228.6 °C for the same fluxes, respectively. Finally, a peak located at 1288.4, 1267.9 and 1286.6 °C for the fluxes B, C and T, respectively. The difference in temperature for these endothermic events can be attributed to the difference in chemical composition of fluxes.

Table 5
Ion content of fluxes

Ion (mol%)	Flux A	Flux B	Flux C	Flux T
Al^{3+}	10.51	14.28	11.01	10.09
Si^{4+}	29.55	22.80	19.79	3.22
Na^{1+}	2.05	3.23	1.15	–
Mn^{2+}	1.17	0.84	2.65	1.36
Mn^{3+}	2.60	1.88	5.90	3.03
Mn^{4+}				
Ti^{2+}	5.5	6.95	2.15	31.79
Ti^{3+}			17.08	
$Ti^{5/3+}$		13.05		
Ca^{2+}	2.34	2.57	2.54	7.64
Mg		1.88		
H^{1+}	0.12	0.03		
F^{1+}				7.26
O^{2+}	46.16	42.21	32.47	35.61

The endothermic reactions corresponding to the above temperatures can be compared with the melting reaction of Gismodine, which has been reported to occur in a temperature range between 965 and 1082 °C. Quartz transformation from Cristobalite to Tridimite occurs between 1200 and 1650 °C. Na_2O sublimation takes place at about 1275 °C. Fluorite and Vesuvianite melt at about 1200 °C. Nefeline melts at temperatures higher than 1248 °C. The melting of corundum, rutile, anastase, hausmannite and quartz was not detected because it occur above 1500 °C.

The zigzag behavior of DTA curves reveals blistering or gassing of the glass formation [15].

3.4. Effect of crystalline phases and ion contents on the behavior of flux

Oxides and carbonates were used for manufacturing the different fluxes. These formed different crystalline phases after sintering. According to the XRD analyses, silica (SiO_2), manganese oxide (MnO) and titanium oxide (TiO_2) were the compounds that reacted during the heating of fluxes.

The silica reacted to form anionic species such as silicates. Three compounds with this characteristic were identified in the sintered fluxes: Nepheline ($NaAlSiO_4$), Gismodine ($CaAl_2Si_2O_8{\cdot}4H_2O$) and Vesuvianite ($Ca_{19}Al_{11}Mg_2Si_{18}O_{69}(OH)_9$).

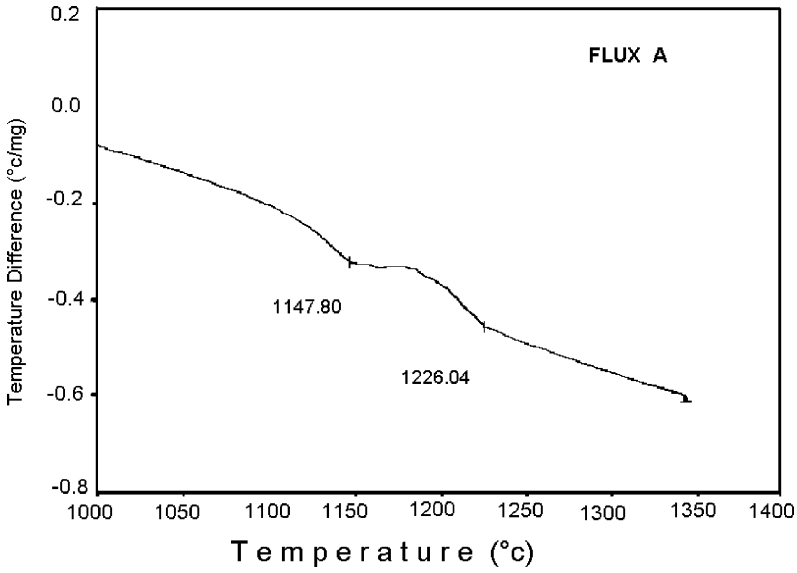

Fig. 5. DTA diagram of flux A.

The silicon electrodeposition in the welding cathodic pool is not as favored as the deposition of volatile calcium from flux. It has been found [14] that a small amount of silicon can be formed electrochemically, but most of it is formed by means of calcium evaporation, which can reduce the SiO_2 in the flux.

It was found that the hausmannite (Mn_3O_4) was formed in the sintered fluxes. This is a spinel with electron valences, Mn^{2+} and Mn^{3+}. Thus, it is possible to have different reactions which permits the formation of several oxide compounds and oxide radicals from MnO, forming inclusions.

The ion quantification determined from the XRD results enables us to estimate the amount of the ions from flux formed in the plasma of electric arc. These ions react with oxygen and the oxides will be deposited on the weld. The most important reactions between the electric arc and welding pool correspond to those where oxygen is involved.

Oxygen can react with any cationic component from the flux, as Na^{1+}, Ca^{2+}, Mg^{2+}, Al^{3+}, Si^{4+}, Fe^{2+}, Fe^{3+}, Mn^{2+}, Mn^{3+}, Mn^{4+}, Ti^{2+}, Ti^{3+}, $Ti^{5/3+}$ and probably $SiO_4{}^{4-}$ from the silicates formed in the fluxes, the anions present are O^{2-} and F^{1-}.

It is possible to make a prediction of the reactions with these cations and anions. Calcium and magnesium are expected to react first with oxygen in the welding arc because its corresponding oxides have the largest negative formation free energy ΔG_f. Al^{3+} has the next highest value

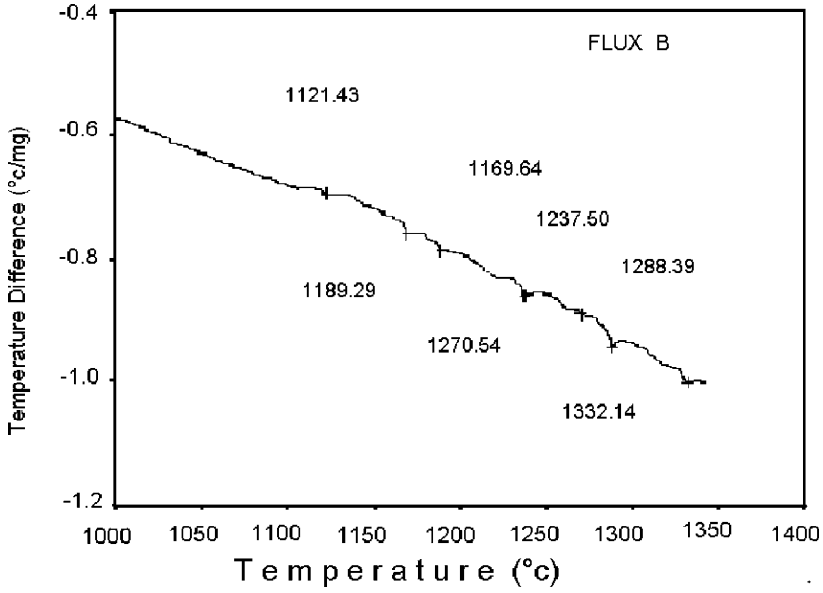

Fig. 6. DTA diagram of flux B.

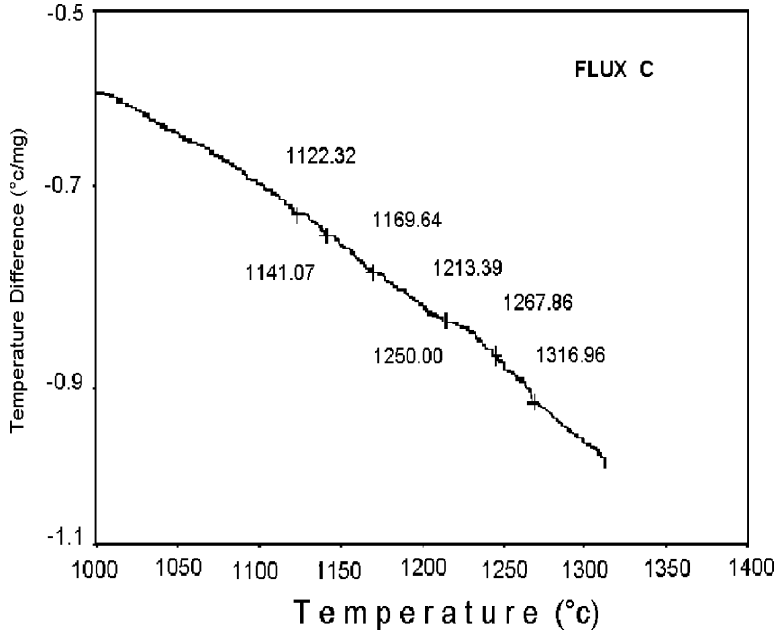

Fig. 7. DTA diagram of flux C.

for the formation of a stable oxide. Si^{4+} and titanium reacts readily with oxygen in the next order. Ti^{2+} almost react at the same time with Mg^{2+}, and then Ti^{3+} and Ti^{4+} react to form stable dioxides to give anions and cations with similar set of reactions. Manganese too exhibit variable valency and may form many oxides and oxide radicals when react with the oxygen in the next order Mn^{2+}, Mn^{3+} and Mn^{4+} in agreement with the corresponding ΔG_f values [14].

The silicates formed will be more soluble in the slag than in the weld pool. Transfer of Mn, Si and Al from the flux to weld pool depends on the amounts in the flux [14]. The oxygen can react with any available cationic species to give non-metallic inclusions. The identification of phases in fluxes can be used to know the behavior of fluxes during their depositing process, as well as the effect of them on the mechanical properties of welds. In the fluxes A, B, C, and T, the presence of corundum can be observed, which has an effect on the facility for slag removing [2]. The same effect has been observed for the presence of rutile in fluxes [2].

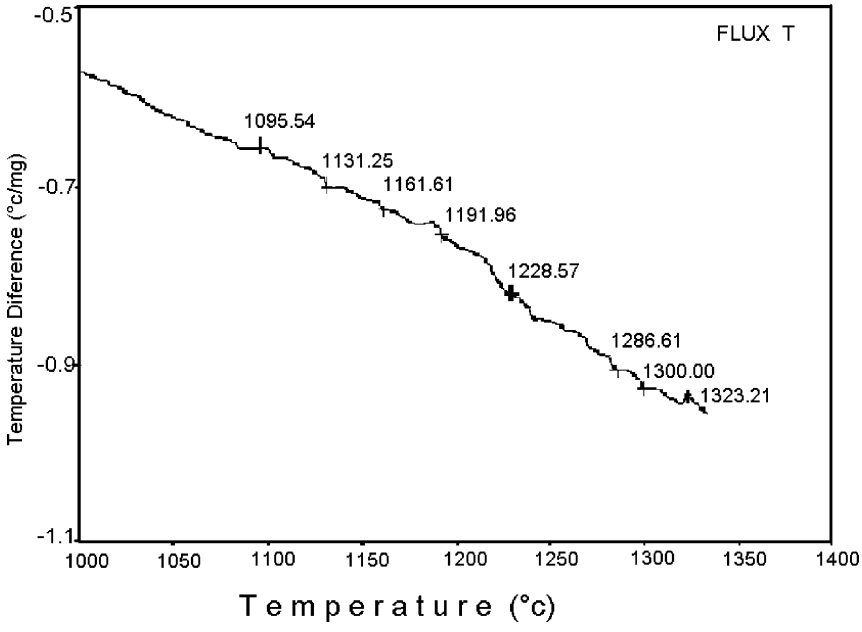

Fig. 8. DTA diagram of flux T.

Calcium ions in fluxes increase the stability of electric arc [16].These ions can come from either oxide or fluoride compounds. A significant calcium content was detected for fluxes A, C and T but not for flux B. Thus, the latter might present an unstable electric arc during welding.

It is also known that quartz and corundum increase the viscosity of fluxes, while the additions of manganese oxide, fluorite and titanium oxide reduce viscosity [2]. The latter compounds were detected in the fluxes A, C, and T, but only a small content, may be as impurity, was observed in the flux B. Thus, a problem of flux fluidity might be present in this flux.

The manganese oxide and quartz have been observed to have a beneficial effect on the mechanical properties of welds [17]. Manganese oxide and quartz were included in the formulation of fluxes A and C, but not for flux B. Titanium oxide has been observed to promote the formation of acicular ferrite, which is less susceptible to cracking [18]. Fluxes C and T are expected to produce the better weld since they contain quartz, manganese oxide, titanium oxide, and the content of oxygen ions (calculated by XRD) is smaller than A and B.

4. Conclusions

The determination of various phases in fluxes enables us to identify the different type of oxides and radicals formed during sintering of the initial materials. This quantification makes it possible to know which anions and cations would be present in the electric arc. The most reactive components react quickly in the weld pool and might be either absorbed in the slag or retained in the weld as inclusions.

Acknowledgements

The authors would like to thank the financial support from FESC-UNAM, CONACYT and CEGEPI-IPN.

References

[1] J.E. Indacochea, M. Blander, S. Shah, Submerged-arc welding: evidence for electrochemical effects on the weld pool, Weld. J. Suppl. Res. 68 (3) (1989) 77–79.
[2] C.E. Jackson, Submerged-arc welding, fluxes and relations among process variables, in: Metals Hand Book, ASM, Metals Park, OH, 1982, pp. 73–77.
[3] S.S. Singer, Industrial Ceramics, Chapman & Hall, London, 1963, pp. 236–257.
[4] A.W. Allen, Optical microscopy in ceramic engineering, in: Proceedings of the Third Berkeley International Materials Conference, Berkeley, CA, June 1966.
[5] R.H. Redwine, M.A. Conrad, Microstructures developed in crystallized glass ceramics, in: Proceedings of the Third Berkeley International Materials Conference, Berkeley, CA, July 1961.
[6] W.B. Dunham, A. Christian, Process Mineralogy of Ceramic Materials, Elsevier, New York, 1984, pp. 20–48.
[7] J.E. Indacochea, S. Shah, Submerged-arc welding: evidence for electrochemical effects on the weld pool, Weld. J. Suppl. Res. 68 (3) (1989) 77–83.
[8] G.R. Belton, T.J. Moore, E.S. Tankins, Slag-metal reactions in submerged-arc welding, Weld. J. Suppl. Res. 42 (7) (1963) 289–290.
[9] N. Christensen, K. Gjermundsen, Measurements of temperature outside and in weld pool in submerged arc welding, US Department of Army, European Research Office, Report No. 273091, 1962.
[10] A. Apold, Carbon Oxidation in the Weld Pool, Pergamon Press, New York, 1962, pp. 33–60.
[11] L.G. Berry, B. Mason, Mineralogy, Freeman, New York, 1959, pp. 150–155.
[12] C. Klein, C.S. Hurbult, Manual of Mineralogy, Wiley, New York, 1999, pp. 566–567.
[13] B.D. Cullity, Elements of X-ray Diffraction, Addison-Wesley, USA, 1978, pp. 407–417.
[14] M.L. Davis, N. Bailey, Evidence from inclusions chemistry of elements transfer during submerged-arc welding, Weld. J. Suppl. Res. 70 (2) (1991) 61–65.
[15] P.K. Gordon, Microstructure of complex ceramics, in: Proceedings of the Third Berkeley International Materials Conference, Berkeley, CA, July 1966.
[16] C.A. Butler, C.E. Jackson, Submerged-arc welding characteristics of the $CaO–TiO_2–SiO_2$ system, Weld. J. Suppl. Res. 46 (10) (1967) 448–456.
[17] J.F. Lancaster, Metallurgy of Welding, Alden Press, London, 1980, pp. 110–177.
[18] G.M. Evans, Microstructure and properties of ferritic steel welds containing Ti and B, Weld. J. Suppl. Res. 75 (8) (1996) 251–259.